© 2019. Published by The Company of Biologists Ltd | Journal of Experimental Biology (2019) 222, jeb206714. doi:10.1242/jeb.206714

SHORT COMMUNICATION

Magnetic resonance imaging (MRI) reveals high cardiac ejection fractions in red-footed tortoises (*Chelonoidis carbonarius*)

Catherine J. A. Williams[1,2,*], Eva M. Greunz[2], Steffen Ringgaard[3], Kasper Hansen[1,4,5], Mads F. Bertelsen[2] and Tobias Wang[1,6]

ABSTRACT

The ejection fraction of the trabeculated cardiac ventricle of reptiles has not previously been measured. Here, we used the gold standard clinical methodology – electrocardiogram-gated flow magnetic resonance imaging (MRI) – to validate stroke volume measurements and end diastolic ventricular blood volume. This produced an estimate of ejection fraction in our study species, the red footed tortoise *Chelonoidis carbonarius* (*n*=5), under isoflurane anaesthesia of 88±11%. After reduction of the prevailing right-to-left intraventricular shunt through the action of atropine, the ejection fraction was 96±6%. This methodology opens new avenues for studying the complex hearts of ectotherms, and validating hypotheses on the function of a more highly trabeculated heart than that of endotherms, which have lower ejection fractions.

KEY WORDS: Ejection fraction, Stroke volume, MRI, Reptile, Trabeculation

INTRODUCTION

The heart serves as a permissive pump providing essential convective blood flow to satisfy the metabolic demands of the body. The substrate for cardiac output (CO) is delivered by the rate of venous return to the heart, and CO is the product of heart rate (f_H) and the volume of blood pumped by each cardiac contraction (stroke volume, V_s). V_s is the difference between end-diastolic volume (EDV) and end-systolic volume (ESV), and animals can therefore increase V_s by elevating EDV and/or by decreasing ESV. Under normal conditions, the ejection fraction (EF) – the proportion of blood ejected in each beat [EF=(EDV−ESV)/EDV] – ranges from 40% to 70% in mammals, meaning that 30–60% of EDV resides in the ventricle at the end of each contraction (Hoffmann et al., 2014; Lang et al., 2015). Similar values apply in birds, although considerably less is known about their cardiac function (Harr et al., 2017; Pees et al., 2004). In contrast to these endothermic hearts, EFs of 80–100% have been measured using echocardiography in fish (Coucelo et al., 2000; Franklin and Davie, 1992; Lai et al., 1998, 2004).

The hearts of most ectothermic vertebrates share the common feature of an extensive proportion of spongy myocardium relative to the compact ventricular wall in mammals and birds (Jensen et al., 2013). It has been speculated that the spongy myocardium of the ectothermic hearts permits pressure development and high EFs with minimal myocardial strain (Johansen, 1965; Shiels and White, 2008). However, while low residual ESV and high EFs have been qualitatively reported for reptiles (Burggren and Johansen, 1982; Millard and Johansen, 1974), quantitative measurements are lacking in the literature. This is probably because it is difficult to acquire sufficiently good images of the spongy myocardium to perform quantitative analyses of EF.

Here, we took advantage of the clinical gold standard human cardiac imaging technique [electrocardiogram (ECG)-gated flow MRI; Hoffmann et al., 2014] to determine flow in the outflow tract of a tortoise, and we validated these measures of V_s by a separate analysis of the dimensions of the ventricle in systole and diastole using biplane and volumetric MRI. In combination with post-mortem measures of cardiac mass (and hence volume of the ventricular tissue), we derived EF. To manipulate CO, we applied atropine to reduce the predominant right-to-left shunt present under isoflurane anaesthesia (Greunz et al., 2018). Our MRI measurements confirm a very high EF in this species, with almost 90% of EDV being pumped by this reptile heart in each beat.

MATERIALS AND METHODS

Animals

Six female red-footed tortoises, *Chelonoidis carbonarius* (Spix 1824), with a body mass of 3.3±0.8 kg (mean±s.d.), were used in the study. The tortoises were group-housed at Aarhus University for 6 months in a 6 m^2 indoor enclosure (26–28°C, 60–80% humidity, 12 h:12 h light:dark cycle) with hiding places, UV lights (160 W UVA+B, Exo Terra, Viborg, Denmark) and heat lamps. There was always access to water and the tortoises were fed daily on mixed vegetables, supplemented by a weekly protein meal. All individuals gained weight, and were deemed healthy based on general clinical examination, white blood cell count, haematocrit and a biochemical profile (Abaxis VetScan VS 2, Scil Animal Care Company GmbH, Viernheim, Germany). Food was withheld 12 h prior to anaesthesia, and procedures were approved by the Danish Experimental Animal Inspectorate (permit no. 2015-15-0201-00684).

In a paired cross-over design, randomized for individual order and treatment (using www.random.org), each tortoise was anaesthetized twice, receiving saline or atropine, separated by a minimum of 5 days. Anaesthesia was induced by inhalation of isoflurane (54±9 min; Vetflurane, VIRBAC, Carros, France; 4–5 ml of isoflurane in 50 l chamber; Bertelsen, 2019) to enable topical application of lidocaine (Xylocaine 20 mg ml^{-1}, AstraZeneca) to the glottis followed by tracheal intubation with an uncuffed tube (2.3–3.5 mm i.d. silicon endotracheal tube). Maintenance was via a semi-closed circle anaesthetic system (Hallowell Small Animal AWS, Pittsfield, MA, USA) with an agent-specific vaporizer

[1]Section of Zoophysiology, Department of Bioscience, Aarhus University, 8000 Aarhus C, Denmark. [2]Center for Zoo and Wild Animal Health, Copenhagen Zoo, Roskildevej 38, 2000 Frederiksberg, Denmark. [3]MR Research Center, Department of Clinical Medicine, Aarhus University, Palle Juul-Jensens Blv. 99, 8200 Aarhus N, Denmark. [4]Comparative Medicine Lab, Department of Clinical Medicine, Aarhus University, Palle Juul-Jensens Blv. 99, 8200 Aarhus N, Denmark. [5]Department of Forensic Medicine, Aarhus University Hospital, Palle Juul-Jensens Blv. 99, 8200 Aarhus N, Denmark. [6]Aarhus Institute of Advanced Sciences, Aarhus University, 8000 Aarhus C, Denmark.

*Author for correspondence (catherine.williams@bios.au.dk)

C.J.A.W., 0000-0002-4839-6134

Received 7 May 2019; Accepted 14 August 2019

Journal of Experimental Biology (2019) 222, jeb206714. doi:10.1242/jeb.206714

List of abbreviations

CO	cardiac output
ECG	electrocardiogram
EDV	end-diastolic volume
EF	ejection fraction
ESV	end-systolic volume
ET_{Iso}	end-tidal isoflurane concentration
f_H	heart rate
MRI	magnetic resonance imaging
V_s	stroke volume

(Ventilator Tec 3, Iso Tec, Ohmeda GR Healthcare, Liverpool, UK) at 4 breaths min^{-1} and a tidal volume of 12.5 ml kg^{-1}; airway pressure at maximum inflation was 12–15 cm H_2O. Atropine (in 0.9% saline, Sigma-Aldrich, 4 mg ml^{-1}) or a matched volume of saline (0.9% sodium chloride, Fresenius Kabi, Uppsala, Sweden) was injected into the jugular vein immediately after intubation. MRI scanning commenced within 43±12 min of injection and lasted 11–39 min (18±8 min).

End-tidal isoflurane concentration (ET_{Iso}), body temperature, respiration rate and heart rate (f_H) were recorded until the animals were placed in the MR-scanner, and again following scanning (equipment: IRMA AX+, Masimo, Sweden Nicolet Elite Doppler, 5 MHz probe, Natus Medical, Inc., Pleasanton, CA, USA). A body temperature of 29–31°C was maintained using an electric heating pad before scanning (Melissa 631-015, Adexi A/S, Skødstrup, Denmark).

MRI safety demands require modification of the ventilation equipment for scanning: longer tubing prefilled with 5% isoflurane was connected to allow uninterrupted mechanical ventilation and anaesthesia from outside the scan room. The tortoises were mechanically ventilated at a vaporizer setting of 5% isoflurane throughout to prohibit movement within the scanner. f_H monitoring was switched to four-limb lead electrocardiogram via non-magnetic clinical attachments, and heating to a digital feedback warm air blower (SAII, Stony Brook, NY, USA). Internal temperature variation between scans of the same individual ranged from 0 to 2.8°C (1.2±1.4°C, mean±s.d.).

MRI measurements: flow determination

Flow was measured as described by Greunz et al. (2018) in a clinical 1.5 T MRI scanner (Philips Healthcare, Amsterdam, The Netherlands), with a head coil as receiver. Anatomical positioning was ascertained via initial localizer scans. Flow measurements orthogonal to the long axis of the heart were derived in the outflow tract using a 7-slice phase-contrast flow sequence (Fig. 1A: slice thickness 4 mm, voxel 0.8×0.8 mm at 27 frames per cardiac cycle with velocity sensitivity parameter 50 cm s^{-1}; Movies 3 and 4). Flow in the right and left pulmonary arteries, left aorta and right aorta or its branches was processed using software (Siswin, Aarhus, Denmark) developed in-house and analysed by two independent observers blind to the administration of atropine. Flow was determined in the first slice above the division of the pulmonary trunk into the left and right pulmonary arteries, where the circular cross-sectional appearance showed that the slice was orthogonal to the artery long axis. Cardiac long-axis views were used to ensure the atropine and saline group slice selection was comparable by confirming the distance from the aortic valves at systole with the slice used for flow measurement (saline distance 7.62±1.79 mm, atropine 7.76±1.5 mm; means±s.d.). The region of interest was manually corrected over each of the vessels, and flow was calculated in each vessel for each heart phase throughout the cardiac cycle (Greunz et al., 2018) (Fig. 1B). Inter-observer error was 6%, regarded as acceptable to justify the flow determination method. The mean of the two observers' measurements was used for flow calculations. In one animal it was not possible to obtain good ECG-gated images, so data from this animal were excluded.

MRI measurements: volume determination

Views of the heart were acquired via an ECG-gated balanced steady-state free precession sequence (slice thickness 2.5 mm and voxel size 0.8×0.8 mm; Movies 1 and 2). The outer circumference of the ventricle and its length (aortic valve to apex), lateral width and breadth (ventral to dorsal) were marked for each cardiac phase (Fig. 1C). Atrial length and area were determined at peak systole and diastole from the slice with the largest atrial dimensions; however, the circumferential area throughout the stack was impossible to reliably determine for each atrium, given their complex shape and surrounding structures.

The images corresponding to peak systole and diastole were determined for each ventricle and separately for the atria, and the volume (v) of the ventricle was calculated from an ellipsoid equation (Eqn 1):

$$v = \frac{4}{3}\pi \cdot 0.5l \cdot 0.5w \cdot 0.5b, \quad (1)$$

where l is length, w is width and b is breadth, and obtained from the sum of slice volumes calculated by multiplying the area of the ventricle in each slice by the slice thickness: v=Σ(slice area×slice thickness). The volume of the atria was estimated as a spheroid based on length and as an ellipsoid based on area in one long-axis image and radius based on atrial length from the same image. Stereological analysis of the ventricles was also attempted using a 5 mm random grid, but although EDV and ESV correlated well with values obtained from slice volume and ellipse measurements, the variability in the data was greater, and this approach was not taken further.

To further validate our methodology, an excised heart from a *Trachemys scripta* (Thunberg in Schoepff 1792) (0.94 kg male, killed with pentobarbital 400 mg kg^{-1} via the subcarapacial sinus) was rinsed and placed in relaxing solution for 2 h (92 mmol l^{-1} NaCl, 4.7 mmol l^{-1} KCl, 1.18 mmol l^{-1} NaH_2PO_4, 20 mmol l^{-1} $MgCl_2$, 1.17 mmol l^{-1} $MgSO_4$, 24 mmol l^{-1} $NaHCO_3$, 5.5 mmol l^{-1} glucose, 2 mmol l^{-1} EGTA, 0.025 mmol l^{-1} EDTA, pH corrected to 7.4 with NaOH; Sigma-Aldrich Denmark A/S, Copenhagen, Denmark). The ventricle was catheterized via the pulmonary trunk, and the outflow tract and atria were tied off with silk (4/0, Kruuse, Langeskov, Denmark). Known volumes of relaxing solution (0.5, 1, 1.5, 2, 3 ml) were injected into the heart and the change in volume was calculated based on the same MRI methods as those used for intact *Chelonoidis carbonarius*. Slice thickness and voxel size were set at half those used in the tortoises, to give the same number of slices within the smaller ventricle. Stereological analysis of this heart using a 5 mm random grid analysed on all slices with over 400 points within the ventricle analysed revealed a good correspondence of volume determined from the MRI (V_d) with volume added (V_a) to the ventricle, V_d=0.9275V_a, with R^2=0.9959.

The mass of the ventricle of the five red-footed tortoises was determined (Sartorius R160P analytical balance) after they were killed with i.v. pentobarbital (400 mg kg^{-1} via the jugular vein) following isoflurane induction. The heart was dissected free of surrounding tissue, placed in heparinized isotonic saline (final concentration 50 IU ml^{-1} from 5000 IU ml^{-1} heparin, Leo Pharma,

Journal of Experimental Biology (2019) 222, jeb206714. doi:10.1242/jeb.206714

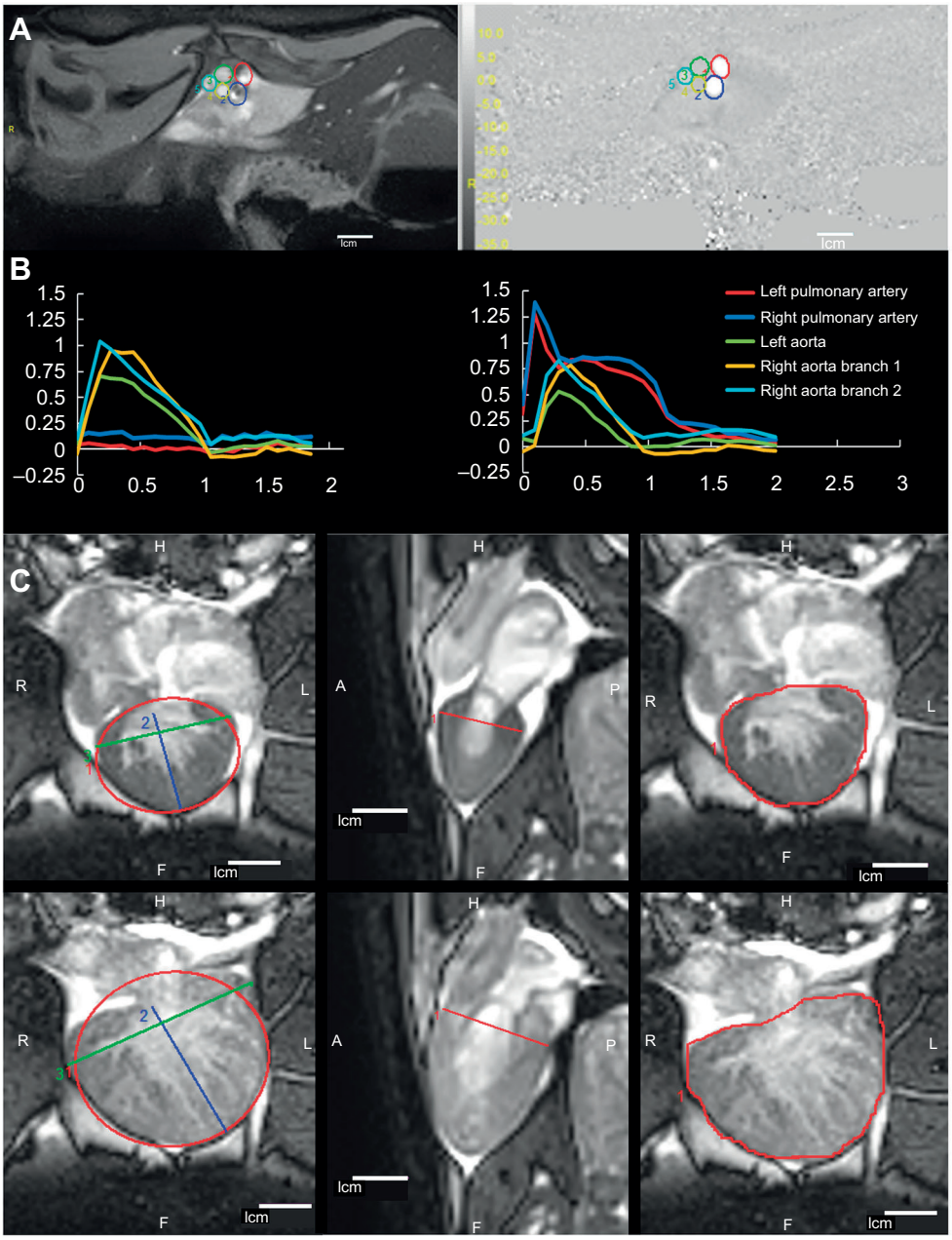

Fig. 1. Electrocardiogram-gated magnetic resonance imaging (MRI) flow and chamber volume determination for a representative individual *Chelonoidis carbonarius*. (A) Modulus and velocity images showing regions of interest placed over the peri-axial plane of the major arteries, orthogonal to flow, during ventricular contraction. The images are from an animal that received atropine, showing early high-velocity flow in the pulmonary arteries (white areas in the velocity image). 1, left pulmonary artery; 2, right pulmonary artery; 3, left aorta; 4, right aorta branch 1; 5, right aorta branch 2. (B) Flow (ml s^{-1} kg^{-1}) over time (s) under isoflurane anaesthesia in saline (left) and atropine (right) treatments, produced from images in A. (Data replotted as mass specific from Greunz et al., 2018, and used to validate calculated values.) (C) Measurements of ventricle volume [ventricular width (green) and length (blue) in the coronal plane in the left column, and breadth (red) in the sagittal plane in the central column, used to calculate volume via the ellipsoid equation] and ventricle perimeter [(red) in the coronal plane, in the right column, used to calculate volume from volume slicing]. Images shown are from peak ventricular systole (upper panel) and diastole (lower panel). H, head/cranial; F, foot/caudal; R, right; L, left; A, anterior/ventral; P, posterior/dorsal.

Ballerup, Denmark; in 0.9% saline, Fresenius Kabi) to aid the dispersion of blood from the chambers, rinsed in further saline, and the ventricle dissected at the atrioventricular border, blotted and weighed. Atria were used for determination of smooth muscle in a parallel study and were therefore not weighed.

The volume of the myocardium was initially calculated both from sedentary mammalian densities and from that used in fish studies, i.e. 1.05 g cm^{-3}, which is also close to the measured value for python ventricular density of 1.068 g cm^{-3} (Franklin and Davie, 1992; Hansen et al., 2012; Vinnakota, 2004) and to the value of 1.00 g cm^{-3} commonly used in chelonian studies, where density is not known directly (e.g. Joyce et al., 2014).

The V_s of the heart was calculated by subtracting images of peak systole from peak diastole and compared with the V_s produced from the flow measurements in the summed individual vessels. The calculated volumes were used to calculate the EF: blood EDV (EDV_{blood}) values could be produced by correcting the measured EDV for the presence of trabeculated spongy muscle within the cardiac silhouette, by subtracting ventricular cardiomyocyte volume as calculated using the mass of the ventricle and a cardiac muscle density of 1.05 mg cm^{-3}. This density assumption and the small measurement error of ventricular mass measurements due to dissection and blotting may account for some measurements of over 100% EF (maximum 103% in one individual) after atropine treatment. Ejection fraction was calculated as:

$$EF = (EDV_{blood} - ESV_{blood})/EDV_{blood} \times 100. \quad (2)$$

Statistical analyses

Paired two-tailed *t*-tests with Welch's correction were used for analysis (De Winter, 2013) in R (http://www.R-project.org/) following Mangiafico (2016). Histograms of difference of paired measurements were inspected to confirm no gross infringement of normality and homoscedasticity; differences were considered

statistically significant at $P<0.05$; effect sizes were considered high at >0.8 (Cohen's *d*); biological relevance is discussed below.

RESULTS AND DISCUSSION

The cardiac cycle was visualized and flow was measured in five intact anaesthetized animals at high temporal resolution (Fig. 1A,B; Movies 1 and 2). In accordance with similar flow measurements using surgically placed blood flow probes (Joyce et al., 2018; Overgaard et al., 2002; Shelton and Burggren, 1976; Wang and Hicks, 1996; White and Ross, 1966), the MRI revealed earlier flow in the pulmonary arteries than in the aortae as a result of the lower afterload (end-diastolic arterial pressure) and the typical prolonged pulmonary flow profile that can be ascribed to high pulmonary compliance (Fig. 1B). EFs in *C. carbonarius* were above 85% (Table 1), which is considerably higher than in mammals, but within the range measured by echocardiography in fish (Franklin and Davie, 1992; Lai et al., 2004).

As in mammalian hearts, the cardiomyocytes of spongy ectothermic hearts shorten by approximately 20% during contraction (Shiels and White, 2008). It is therefore believed that the very high EF of the ectothermic vertebrate heart is possibly due to the effective nature of many small chambers within the spongy myocardium, which can generate pressure and be almost completely emptied (Burggren et al., 2014) without a large strain on the myocytes as a result of Laplace's law (Johansen, 1965).

Calculated V_s using slice volume and ellipsoid equation methods corresponded well to measured flow volume in all individuals, and to injected volumes in the excised *Trachemys* heart (Fig. 2). In the excised relaxed heart, the volume contained by the ventricle at zero filling pressure was 0.95–1.5 ml solution kg^{-1} body mass, or 0.86–1.37 ml solution g^{-1} ventricle mass. In the excised heart and *in vivo*, disc-based volumes were significantly higher than those calculated from the ellipsoid equation, probably partly due to partial volume effects. In this case, biplane MRI provided the best correlation with flow measurements when the intercept was not constrained (R^2 ellipse=0.93, R^2 disc=0.85) given lower variability, while with the intercept constrained to 0, the regression for volumetric measurement lay closer to the line of identity (Fig. 2). Previous reports revealed some disparity between biplane and volumetric measurements in axolotls and humans using echocardiography or MRI, with a tendency to obtain smaller EFs with volumetric measurements in comparison with biplane measurements (Chuang et al., 2000; Gomes et al., 2018). This was also the case in our study, where volumetric measurements led to slightly, but statistically significantly lower EFs (81±12% and 87±8% after atropine). Although the values of cardiac flow were statistically different from those obtained by the ellipsoid equation, the results show that the biological significance of method choice was low at the COs studied here. As shown in Fig. 2, the regressions for the volumes produced by the two methods diverge slightly at higher blood flows. Volumetric measurements are more difficult in smaller hearts because of the partial volume effect, and greater resolution scans may be required with specimens smaller than those studied here. EF, as expected, remained very high after atropine although EDV increased as a result of the increased rate of venous return from the pulmonary circulation.

Mass-adjusted V_s (Table 1) after atropine was similar to the 3.3±0.3 and 3.07±0.69 ml kg^{-1} min^{-1} recorded during ventilation or physical activity in recovered *Trachemys scripta* and *Testudo graeca* (Joyce et al., 2018; Krosniunas and Hicks, 2003; Shelton and Burggren, 1976). V_s, however, was lower in our isoflurane-anaesthetized tortoises without atropine than in the apnoeic or diving conscious chelonians described in those studies, but similar to that in pentobarbital-anaesthetized *Trachemys* (e.g. Comeau and Hicks, 1994). f_H at 30°C was similar to that previously reported for conscious chelonians allowing for Q_{10} effects of body temperature (Johnson et al., 2008; Joyce et al., 2018; Kinney et al., 1977; Kischinovsky et al., 2013; Krosniunas and Hicks, 2003; Shelton and Burggren, 1976; Wang and Hicks, 1996), and lower than that of pentobarbital-anaesthetized or extensively handled animals

Table 1. Cardiac parameters for isoflurane-anaesthetized *Chelonoidis carbonarius* treated with saline or atropine

	Saline	Atropine	*P*-value
Ventricle mass (g)	4.67±0.83		
f_H (beats min^{-1})	30±5	30±2	1
Ventricular parameters relative to body mass			
Ventricular mass (g kg^{-1})	1.38±0.18		
$V_{s,flow}$ (ml kg^{-1})	1.93±0.38	3.15±0.67	0.001965
EDV blood (ml kg^{-1})	1.99±0.48	3.14±0.63	0.002256
ESV blood (ml kg^{-1})	0.23±0.20	0.12±0.19	0.220571
$V_{s,calculated}$ (ml kg^{-1})	1.76±0.47	3.02±0.69	0.005233
CO ($f_H \times V_{s,flow}$) (ml kg^{-1} min^{-1})	56.99±9.28	94.89±22.33	0.022597
EF (%)	88.37±10.61	96.05±6.08	0.137617
Atrial parameters relative to body mass			
Right atrial volume (diastole, ml kg^{-1})	1.50±0.80	2.59±1.06	
Right atrial volume (systole, ml kg^{-1})	0.41±0.30	0.79±0.44	
Right atrial V_s (ml kg^{-1})	1.09±0.64	1.80±0.72	
Left atrial volume (diastole, ml kg^{-1})	0.63±0.29	1.36±0.92	
Left atrial volume (systole, ml kg^{-1})	0.24±0.13	0.31±0.13	
Left atrial V_s (ml kg^{-1})	0.39±0.22	1.04±0.81	

Data are means±s.d., calculated using the ellipse method. *P*-values are reported for paired two-tailed *t*-test. *n*=5.
V_s, stroke volume obtained from flow or calculated; EDV, end-diastolic volume; ESV, end-systolic volume; CO, cardiac output; EF, ejection fraction.

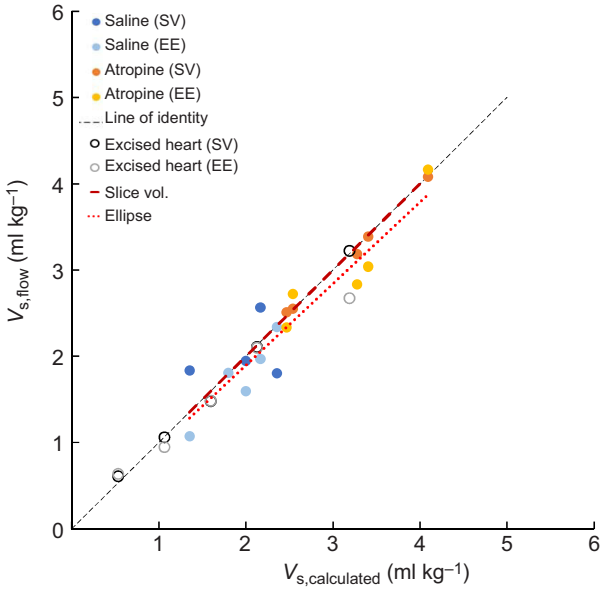

Fig. 2. Verification of calculated stroke volume (V_s) using flow measurements. Calculated V_s plotted against measured V_s (from outflow tract flow or injected volume) for atropine-treated (1 mg kg^{-1}; yellow circles) and saline-treated (blue circles) *C. carbonarius* (*n*=5) and an excised heart from *Trachemys scripta* (*n*=1; open circles). Darker symbols are those where volume was calculated via slice volume (SV) measurements, lighter symbols correspond to the use of the ellipsoid equation (EE). A line of identity and regression lines for the use of slice volume measurements and the ellipsoid equation, all with the intercept constrained to 0, are indicated.

(Cermakova et al., 2018; Comeau and Hicks, 1994; Crossley et al., 1998; Joyce et al., 2018). The failure of atropine to increase f_H was unexpected, particularly given the marked effects on the pulmonary circulation that also obey an inhibitory vagal influence (Burggren, 1975), and may be attributed to the isoflurane anaesthesia. It is possible that the direct cardio-depressive effect of isoflurane may have lowered the EF (Housmans et al., 2000; Murray et al., 1989). Alternatively, or in addition, isoflurane may have reduced the afterload (through arterial hypotension), which could increase EF compared with that in conscious tortoises, given the steep negative relationship between V_s and afterload in chelonians (Farrell et al., 1994; Joyce et al., 2016). Measurements were taken at 60 min of anaesthesia, under presumed steady state, but any effect of isoflurane on EF and CO may have been magnified in the atropine group if atropine, by reducing the right-to-left shunt, led to a greater arterial concentration of isoflurane. Measurements of arterial and venous pressure would enable a disentangling of the effects of atropine, isoflurane and central and peripheral vascular effects of the anaesthetic on EF.

Atropine caused the expected rise in pulmonary blood flow. The rise in pulmonary venous return increased EDV and resulted in a doubling of CO (saline versus atropine P=0.023) with an elimination of the net right-to-left shunt seen under isoflurane anaesthesia alone as reported in our earlier study (Greunz et al., 2018). Only tentative conclusions can be drawn from our atrial measurements given the great variation in shape observed in the MRI within the studied individuals, but the most concrete measure is of atrial length. In the right atrium, little change was observed in the length and calculated V_s of the atria following treatment with atropine; however, there was a tendency for increased V_s of the left atrium after atropine, consistent with increased pulmonary venous return. The measured CO under saline and atropine was similar to previous reports in chelonia during apnoea and ventilation, or rest and activity, respectively (Joyce et al., 2018; Krosniunas and Hicks, 2003; Shelton and Burggren, 1976). Larger disparities in CO have been reported in some experimental dives in *Trachemys* (Wang and Hicks, 1996; White and Ross, 1966). In conclusion, ECG-gated MRI can provide high-resolution data for analysis of the cardiac cycle in complex cardiovascular systems, and here allows us to present the first measurement of high EFs in a reptile.

Acknowledgements
We gratefully acknowledge the excellent animal care of Heidi Meldgaard Jensen and Claus Wandborg, and the helpful contributions of anonymous reviewers to the final manuscript.

Competing interests
The authors declare no competing or financial interests.

Author contributions
Conceptualization: C.J.A.W., E.M.G., S.R., K.H., M.F.B., T.W.; Methodology: C.J.A.W., E.M.G., S.R., K.H., T.W.; Software: S.R.; Validation: S.R.; Formal analysis: C.J.A.W., S.R., K.H.; Investigation: C.J.A.W., E.M.G.; Data curation: C.J.A.W.; Writing - original draft: C.J.A.W.; Writing - review & editing: C.J.A.W., E.M.G., S.R., K.H., M.F.B., T.W.; Visualization: C.J.A.W.; Supervision: S.R., M.F.B., T.W.; Project administration: C.J.A.W., M.F.B., T.W.; Funding acquisition: C.J.A.W., M.F.B., T.W.

Funding
C.J.A.W. gratefully acknowledges funding from the Novo Nordisk Foundation, E.M.G. is funded by a grant from the Annie and Otto Johs. Detlefs' Foundation, and T.W. is funded by the Danish Council for Independent Research, Natural Sciences (Det Frie Forskningsråd | Natur og Univers, FNU).

Supplementary information
Supplementary information available online at
http://jeb.biologists.org/lookup/doi/10.1242/jeb.206714.supplemental

References
Bertelsen, M. F. (2019). Anaesthesia and analgesia. In *BSAVA Manual of Reptiles*, pp. 200-209. British Small Animal Veterinary Association.

Burggren, W. W. (1975). A quantitative analysis of ventilation tachycardia and its control in two chelonians, Pseudemys scripta and Testudo graeca. *J. Exp. Biol.* **63**, 367-380.

Burggren, W. and Johansen, K. (1982). Ventricular haemodynamics in the monitor lizard varanus ex anthematicus: pulmonary and systemic pressure separation. *J. Exp. Biol.* **96**, 343-354.

Burggren, W. W., Christoffels, V. M., Crossley, D. A., Enok, S., Farrell, A. P., Hedrick, M. S., Hicks, J. W., Jensen, B., Moorman, A. F. M., Mueller, C. A. et al. (2014). Comparative cardiovascular physiology: future trends, opportunities and challenges. *Acta Physiol.* **210**, 257-276. doi:10.1111/apha.12170

Cermakova, E., Ceplecha, V. and Knotek, Z. (2018). Efficacy of two methods of intranasal administration of anaesthetic drugs in red-eared terrapins (Trachemys scripta elegans). *Vet. Med. (Praha).* **63**, 87-93. doi:10.17221/74/2017-VETMED

Chuang, M. L., Hibberd, M. G., Salton, C. J., Beaudin, R. A., Riley, M. F., Parker, R. A., Douglas, P. S. and Manning, W. J. (2000). Importance of imaging method over imaging modality in noninvasive determination of left ventricular volumes and ejection fraction: assessment by two- and three-dimensional echocardiography and magnetic resonance imaging. *J. Am. Coll. Cardiol.* **35**, 477-484. doi:10.1016/S0735-1097(99)00551-3

Comeau, S. G. and Hicks, J. W. (1994). Regulation of central vascular blood flow in the turtle. *Am. J. Physiol. Integr. Comp. Physiol.* **267**, R569-R578. doi:10.1152/ajpregu.1994.267.2.R569

Coucelo, J., Joaquim, N. and Coucelo, J. (2000). Calculation of volumes and systolic indices of heart ventricle from Halobatrachus didactylus: echocardiographic noninvasive method. *J. Exp. Zool.* **286**, 585-595. doi:10.1002/(SICI)1097-010X(20000501)286:6<585::AID-JEZ5>3.0.CO;2-Z

Crossley, D., Altimiras, J. and Wang, T. (1998). Hypoxia elicits an increase in pulmonary vasculature resistance in anaesthetised turtles (Trachemys scripta). *J. Exp. Biol.* **201**, 3367-3375.

De Winter, J. C. F. (2013). Using the student's *t*-test with extremely small sample sizes. *Pract. Assessment, Res. Eval.* **18**. http://pareonline.net/getvn.asp?v=18&n=10

Farrell, A. P., Franklin, C. E., Arthur, P. G., Thorarensen, H. and Cousins, K. L. (1994). Mechanical performance of an *in-situ* perfused heart from the turtle chrysemys scripta during normoxia and anoxia at 5-degrees-c and 15-degrees-C. *J. Exp. Biol.* **191**, 207-229.

Franklin, C. E. and Davie, P. S. (1992). Dimensional analysis of the ventricle of an in situ perfused trout heart using echocardiography. *J. Exp. Biol.* **166**, 47-60.

Gomes, L., Veld, O., Graaf, D., Sanches, P. G., Roel, C., De Graaf, W. and Strijkers, G. J. (2018). Novel axolotl cardiac function analysis method using magnetic resonance imaging. *PLoS ONE* **12**, 1-15. doi:10.1371/journal.pone.0183446

Greunz, E. M., Williams, C. J., Ringgaard, S., Hansen, K., Wang, T. and Bertelsen, M. F. (2018). Elimination of intracardiac shunting provides stable gas anesthesia in tortoises. *Sci. Rep.* **8**, 17124. doi:10.1038/s41598-018-35588-w

Hansen, K., Pedersen, P. B. M., Pedersen, M. and Wang, T. (2012). Magnetic resonance imaging volumetry for noninvasive measures of phenotypic flexibility during digestion in burmese pythons. *Physiol. Biochem. Zool.* **86**, 149-158. doi:10.1086/668915

Harr, K. E., Rishniw, M., Rupp, T. L., Cacela, D., Dean, K. M., Dorr, B. S., Hanson-Dorr, K. C., Healy, K., Horak, K., Link, J. E. et al. (2017). Dermal exposure to weathered MC252 crude oil results in echocardiographically identifiable systolic myocardial dysfunction in double-crested cormorants (Phalacrocorax auritus). *Ecotoxicol. Environ. Saf.* **146**, 76-82. doi:10.1016/j.ecoenv.2017.04.010

Hoffmann, R., Barletta, G., Von Bardeleben, S., Vanoverschelde, J. L., Kasprzak, J., Greis, C. and Becher, H. (2014). Analysis of left ventricular volumes and function: a multicenter comparison of cardiac magnetic resonance imaging, cine ventriculography, and unenhanced and contrast-enhanced two-dimensional and three-dimensional echocardiography. *J. Am. Soc. Echocardiogr.* **27**, 292-301. doi:10.1016/j.echo.2013.12.005

Housmans, P. R., Wanek, L. A., Carton, E. G. and Bartunek, A. E. (2000). Effects of halothane and isoflurane on the intracellular Ca2+ transient in ferret cardiac muscle. *Anesthesiology* **93**, 189-201. doi:10.1097/00000542-200007000-00030

Jensen, B., Wang, T., Christoffels, V. M. and Moorman, A. F. M. (2013). Evolution and development of the building plan of the vertebrate heart. *Biochim. Biophys. Acta Mol. Cell Res.* **1833**, 783-794. doi:10.1016/j.bbamcr.2012.10.004

Johansen, K. (1965). Cardiovascular dynamics in fishes, amphibians and reptiles. *Ann. N. Y. Acad. Sci.* **127**, 414-442. doi:10.1111/j.1749-6632.1965.tb49417.x

Johnson, S. M., Kinney, M. E. and Wiegel, L. M. (2008). Inhibitory and excitatory effects of micro-, delta-, and kappa-opioid receptor activation on breathing in awake turtles, Trachemys scripta. *Am. J. Physiol. Regul. Integr. Comp. Physiol.* **295**, R1599-R1612. doi:10.1152/ajpregu.00020.2008

Joyce, W., Gesser, H. and Wang, T. (2014). Purinoceptors exert negative inotropic effects on the heart in all major groups of reptiles. *Comp. Biochem. Physiol. A Mol. Integr. Physiol.* **171**, 16-22. doi:10.1016/j.cbpa.2014.02.005

Joyce, W., Axelsson, M., Altimiras, J. and Wang, T. (2016). *In situ* cardiac perfusion reveals interspecific variation of intraventricular flow separation in reptiles. *J. Exp. Biol.* **219**, 2220-2227. doi:10.1242/jeb.139543

Joyce, W., Williams, C. J. A., Crossley, D. A. and Wang, T. (2018). Venous pressures and cardiac filling in turtles during apnoea and intermittent ventilation. *J. Comp. Physiol. B Biochem. Syst. Environ. Physiol.* **188**, 481-490. doi:10.1007/s00360-017-1132-3

Kinney, J. L., Matsuura, D. T. and White, F. N. (1977). Cardiorespiratory effects of temperature in the turtle, Pseudemys floridana. *Respir. Physiol.* **31**, 309-325. doi:10.1016/0034-5687(77)90074-3

Kischinovsky, M., Duse, A., Wang, T. and Bertelsen, M. F. (2013). Intramuscular administration of alfaxalone in red-eared sliders (Trachemys scripta elegans)–effects of dose and body temperature. *Vet. Anaesth. Analg.* **40**, 13-20. doi:10.1111/j.1467-2995.2012.00745.x

Krosniunas, E. H. and Hicks, J. W. (2003). Cardiac output and shunt during voluntary activity at different temperatures in the turtle, trachemys scripta. *Physiol. Biochem. Zool.* **76**, 679-694. doi:10.1086/377745

Lai, N. C., Graham, J. B., Dalton, N., Shabetai, R. and Bhargava, V. (1998). Echocardiographic and hemodynamic determinations of the ventricular filling pattern in some teleost fishes. *Physiol. Zool.* **71**, 157-167. doi:10.1086/515901

Lai, N. C., Dalton, N., Yin, Y., Kwong, C., Rasmussen, R., Holts, D. and Graham, J. B. (2004). A comparative echocardiographic assessment of ventricular function in five species of sharks. *Comp. Biochem. Physiol. A Mol. Integr. Physiol.* **137**, 505-521. doi:10.1016/j.cbpb.2003.11.011

Lang, R. M., Badano, L. P., Mor-Avi, V., Afilalo, J., Armstrong, A., Ernande, L., Flachskampf, F. A., Foster, E., Goldstein, S. A., Kuznetsova, T. et al. (2015). Recommendations for cardiac chamber quantification by echocardiography in adults: an update from the American society of echocardiography and the European association of cardiovascular imaging. *Eur. Heart J. Cardiovasc. Imaging* **16**, 233-271. doi:10.1093/ehjci/jev014

Mangiafico, S. S. (2016). *Summary and Analysis of Extension Program Evaluation in R, version 1.15.0*. New Brunswick, NJ: Rutgers Cooperative Extension.

Millard, R. W. and Johansen, K. (1974). Ventricular outflow dynamics in the lizard, Varanus niloticus: responses to hypoxia, hypercarbia and diving. *J. Exp. Biol.* **60**, 871-880.

Murray, D. J., Forbes, R. B., Dillman, J. B., Mahoney, L. T. and Dull, D. L. (1989). Haemodynamic effects of atropine during halothane or isoflurane anaesthesia in infants and small children. *Can. J. Anaesth.* **36**, 295-300. doi:10.1007/BF03010768

Overgaard, J., Stecyk, J. A. W., Farrell, A. P. and Wang, T. (2002). Adrenergic control of the cardiovascular system in the turtle Trachemys scripta. *J. Exp. Biol.* **205**, 3335-3345.

Pees, M., Straub, J. and Krautwald-Junghanns, M.-E. (2004). Echocardiographic examinations of 60 African grey parrot snd 30 other psittacine birds. *Vet. Rec.* **155**, 73-77. doi:10.1136/vr.155.3.73

Shelton, G. and Burggren, W. (1976). Cardiovascular dynamics of the chelonia during apnoea and lung ventilation. *J. Exp. Biol.* **64**, 323-343.

Shiels, H. A. and White, E. (2008). The Frank-Starling mechanism in vertebrate cardiac myocytes. *J. Exp. Biol.* **211**, 2005-2013. doi:10.1242/jeb.003145

Vinnakota, K. C. (2004). Myocardial density and composition: a basis for calculating intracellular metabolite concentrations. *AJP Hear. Circ. Physiol.* **286**, H1742-H1749. doi:10.1152/ajpheart.00478.2003

Wang, T. and Hicks, J. W. (1996). Cardiorespiratory synchrony in turtles. *J. Exp. Biol.* **199**, 1791-1800.

White, F. N. and Ross, G. (1966). Circulatory changes during experimental diving in the turtle. *Am. J. Physiol.* **211**, 15-18. doi:10.1152/ajplegacy.1966.211.1.15

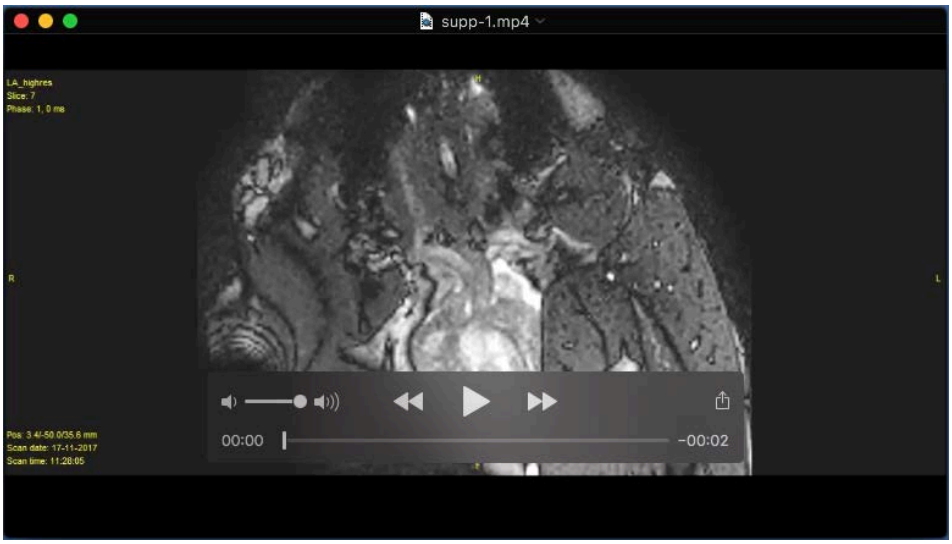

Movie 1. Coronal long axis view.

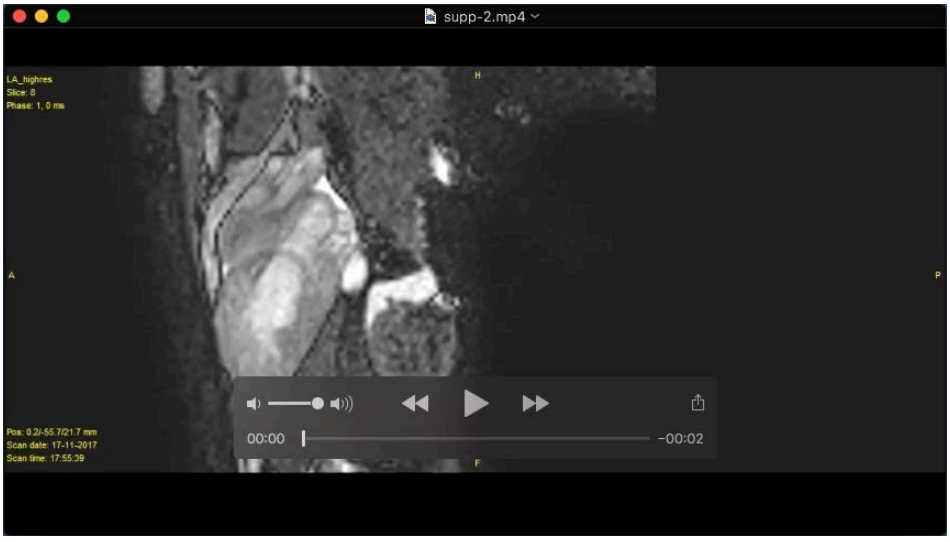

Movie 2. Sagittal long axis view.

Journal of Experimental Biology • Supplementary information

Movie 3. Cross-sectional flow measurements in the tortoise cardiac outflow tract. Slice thickness 4 mm, voxel 0.8×0.8 mm at 27 frames per cardiac cycle with velocity sensitivity parameter 50 cm s^{-1}. See Fig. 1 for key to vessel identity.

Movie 4. Cross-sectional images: velocity determination in the cardiac outflow tract. Slice thickness 4 mm, voxel 0.8×0.8 mm at 27 frames per cardiac cycle with velocity sensitivity parameter 50 cm s^{-1}. See Fig. 1 for key to vessel identity.